Article

Ultra-narrow linewidth polarization-insensitive filter using a symmetry-breaking selective plasmonic metasurface

Yash D Shah, James Grant, Danni Hao, Mitchell Kenney, Vincenzo Pusino, and David R.S. Cumming

ACS Photonics, **Just Accepted Manuscript** • DOI: 10.1021/acsphotonics.7b01011 • Publication Date (Web): 12 Dec 2017

Ultra-narrow linewidth polarization-insensitive filter using a symmetry-breaking selective plasmonic metasurface

Yash D. Shah,* James Grant, Danni Hao, Mitchell Kenney, Vincenzo Pusino, and David R. S. Cumming*

Microsystems Technology group, Electronics and Nanoscale engineering, Department of Engineering, University of Glasgow, Glasgow, UK.

E-mail: YashDiptesh.Shah@glasgow.ac.uk; david.cumming.2@glasgow.ac.uk

Abstract

Plasmonic metasurfaces provide unprecedented control of the properties of light. By designing symmetry-breaking nanoholes in a metal sheet and engineering the optical properties of the metal using geometry, highly selective transmission and polarisation control of light is obtained. To date such plasmonic filters have exhibited broad (> 200 nm) transmission linewidths in the NIR and as such are unsuitable for applications requiring narrow passbands, e.g. multi-spectral imaging. Here we present a novel sub-wavelength elliptical and circular nanohole array in a metallic film that simultaneously exhibits high transmission efficiency, polarisation insensitivity and narrow linewidth. The experimentally obtained linewidth is 79 nm with a transmission efficiency of 44%. By examining the electric and magnetic field distributions for various incident polarisations at the transmission peak we show that the narrowband characteristics are due

*To whom correspondence should be addressed

to a Fano resonance. Good agreement is obtained between the experimental data, simulations and analytical calculations. Our design can be modified to operate in other regions of the electromagnetic spectrum and these filters may be integrated with suitable detectors such as photodiodes and single photon avalanche diode (SPAD) arrays.

Keywords: (plasmonics; Fano resonance; metasurface; nanophotonics; surface plasmon polaritons; subwavelength optics)

Nanophotonics encompasses a broad field that deals with quantum and classical light-matter interaction that can yield devices used for applications such as imaging,[1–3] spectroscopy and bio-sensing.[4–6] In recent years significant progress has been made in nanophotonics based on the phenomena of surface plasmon resonance[7,8] and plasmonic metasurfaces.[9–12] There has been growing interest in these two-dimensional metasurfaces,[13–17] since their introduction, for manipulating the propagation of electromagnetic waves.[18] The thickness of these structures is far smaller than the operational wavelength, which allows the miniaturization and integration of various optical components and systems. Plasmonic metasurfaces have gained prominence in this field due to their ability to control individually and simultaneously the phase,[19] momentum,[20] amplitude[21] and polarization of light[19] and hence promise great utility in the realization of compact photonic devices through tuneable resonant properties controlled by near field coupling.[22] In addition, there has been particular interest in ultrathin metasurfaces operating in transmission mode, but these metasurfaces are still in their infancy because of their low efficiency.

The periodic arrangement of nanoholes in a metal sheet leads to resonant coupling between the surface plasmon polaritons (SPP) on the surface of the corrugated metal surface and the incident light leading to extraordinary optical transmission (EOT).[22–28] It has been demonstrated that both the period and the geometry of the nanoholes (localised surface plasmon resonance) play a role in determining the transmission characteristics.[22] Plasmonic filters consist of circular or rectangular nanoholes[21,22,29–31] or gratings in a thin metal film arranged in a periodic array.[23,32,33] Such plasmonic bandpass filters are a simple and elegant

alternative to the more complex and challenging to fabricate dichroic film filters. Moreover, the resonance transmission passband of a plasmonic metasurface filter can be shifted to a desired frequency by altering the size and period of the nanoholes. Although the use of metals results in losses in the SPP, several strategies have been presented to overcome this deficiency.[7,34] For a single layer filter with a regular triangular circular hole lattice on glass, the transmission observed was between 30-35% with a linewidth of >100 nm in the visible spectrum.[30] Similar devices made in the near infrared (NIR) region achieved a transmission coefficient of 65%[31] with a broad linewidth of 220 nm. High transmission has been observed for multilayer Fabry-Prot type designs (multiple stacks of alternating metallic and dielectric structures) that increase the transmission coefficient to 60-65% with a linewidth of 110 nm in the visible.[35] These designs, however, generally require sophisticated fabrication processes and complicated variations of unit cells. The combination of high transmission and narrow linewidth has to date proved difficult to achieve. Moreover, plasmonic filters typically suffer from poor out-of-band suppression with unwanted transmission peaks observed at longer wavelengths. Narrow linewidth, high transmission efficiency, low-cost and miniaturizable filters suitable for monolithic integration with detectors are desirable for multispectral imaging applications as well as gas detection due to the narrow spectral response of molecules such as CO, NO and CH_4.[35,36]

Results and discussion

In this letter we present a novel NIR filter yielding high transmission, narrow linewidth, and polarisation insensitivity using an array, wherein elliptical nanoholes are made alongside circular ones, with a hexagonal lattice to form a supercell. An advantage of this design is that because it is a single layer fabrication process, it can be tuned to any desirable wavelength by scaling the elliptical and circular nanohole sizes and period. Hexagonal lattice arrangements of nanoholes have been shown to provide sharper EOT resonances and a higher confinement of

E-field which make this arrangement suitable for sensing applications.[37,38] Elliptical nanohole arrays[39,40] have been investigated to provide an efficient polarisation dependent,[41] broadband response[42,43] and have found applications in biosensing due to the high sensitivity to changes in refractive index.[44] Two designs are presented in our investigation, the unit cells of which are highlighted in Figure 1. In the first instance we have a design optimised with ellipses oriented all at the same angle of 135° to the x-axis, as shown in Figure 1(A)(i), and in the second instance we have a design with ellipses alternately oriented in 45° and 135°, as shown in Figure 1(A)(ii) .

Due to the permittivity discontinuity at metal-dielectric surfaces, SPPs have an in-plane momentum. Under normally incident light, the free-space radiation cannot couple to surface plasmons directly but it is feasible, with the help of a grating, to provide the additional momentum. The SPP momentum vector is given by, $\boldsymbol{k}_{spp}=\boldsymbol{k}_{sin\theta}+\boldsymbol{k}_{i,j}$, where $\boldsymbol{k}_{sin\theta}$ is the momentum from light incident on the device and $\boldsymbol{k}_{i,j}$ is dependent on the diffraction grating order. For normally incident light, $\boldsymbol{k}_{sin\theta}$ is 0 and hence $\boldsymbol{k}_{spp}$ is given as Equation 1;

$$k_{spp} = k_{i,j} = \frac{a^*}{\sqrt{\frac{4}{3}(i^2+ij+j^2)}}\sqrt{\frac{\varepsilon_m\varepsilon_d}{\varepsilon_m+\varepsilon_d}} \quad (1)$$

where a^* is the period of the nanoholes in the metal sheet, (i,j) signify the diffraction grating order and ϵ_m and ϵ_d are the permittivities of metal and dielectric respectively. To obtain a value of $\boldsymbol{k}_{spp}$ corresponding to a transmission minimum[45,46] of 1.52 μm we calculated that the lattice period a^* should be 1.17 μm for the (1,0) diffraction order.

The thickness of the gold was selected to be 80 nm as it gave a good trade-off between linewidth and transmission for the calculated period (See Figure S1 in the Supplementary information). The ratio of the short axis to long axis (b/a) of the ellipses was selected to be 0.8. Figure 1(B) shows the variation in simulated transmission spectrum for the design with ellipses orientated at 45° and 135°. The linewidths for several b/a ratios are also labelled. Assuming an E-field dependency such that $(\boldsymbol{E}_b/\boldsymbol{E}_a)^2 \propto$ (b/a), $\boldsymbol{E}_a$ and $\boldsymbol{E}_b$ should

be approximately equal for b/a ratios in the range 0.75 - 0.85.[41] Owing to subwavelength confinement of the E-field mode, the dimensions of the nanoholes were limited to $\lambda/4$. The dimensions of the ellipses were 430 nm by 346 nm (long axis and short axis respectively with a b/a ratio of 0.8) and the circles have a diameter of 404 nm. A 300 nm thick cap layer of SiO_2 was deposited on the perforated metal layer.

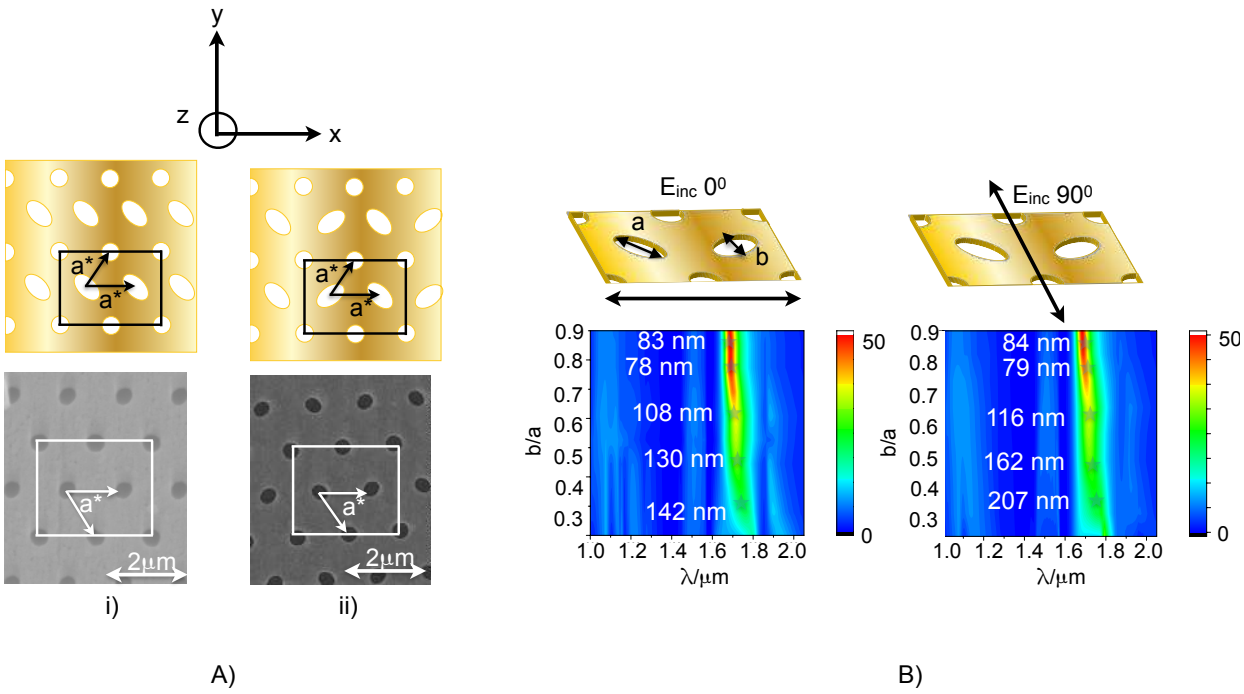

Figure 1: (A)(i) and (ii) Schematic and the corresponding SEM images of two plasmonic metasurfaces with elliptical and circular nanoholes arranged periodically. a^* is the period. (B) For $\boldsymbol{E}_{inc}$ at 0° and 90° polarisations, the transmission spectra were simulated as a function of the ratio: b/a i.e. ratio of short axis to long axis. It can be seen seen from the dispersion colour plots that the linewidth narrows with increasing b/a in the range 0.3 – 0.9.

The fabrication of these devices is described in the Methods section. The transmission spectra were measured in a CRAIC 20/30 PV^{TM} micro-photo-spectrometer system with a polariser and condenser lens. The aperture for the incident light has a diameter of 0.5 mm and the objective lens has a NA of 0.25.

Figure 2 plots the transmission spectra measured from the designs with unit cell highlighted in the SEM insets. Figure 2(A), shows the experimental transmission spectrum for the design with the ellipses oriented at 135° for incident light polarised at 0°, 45°, 90° and

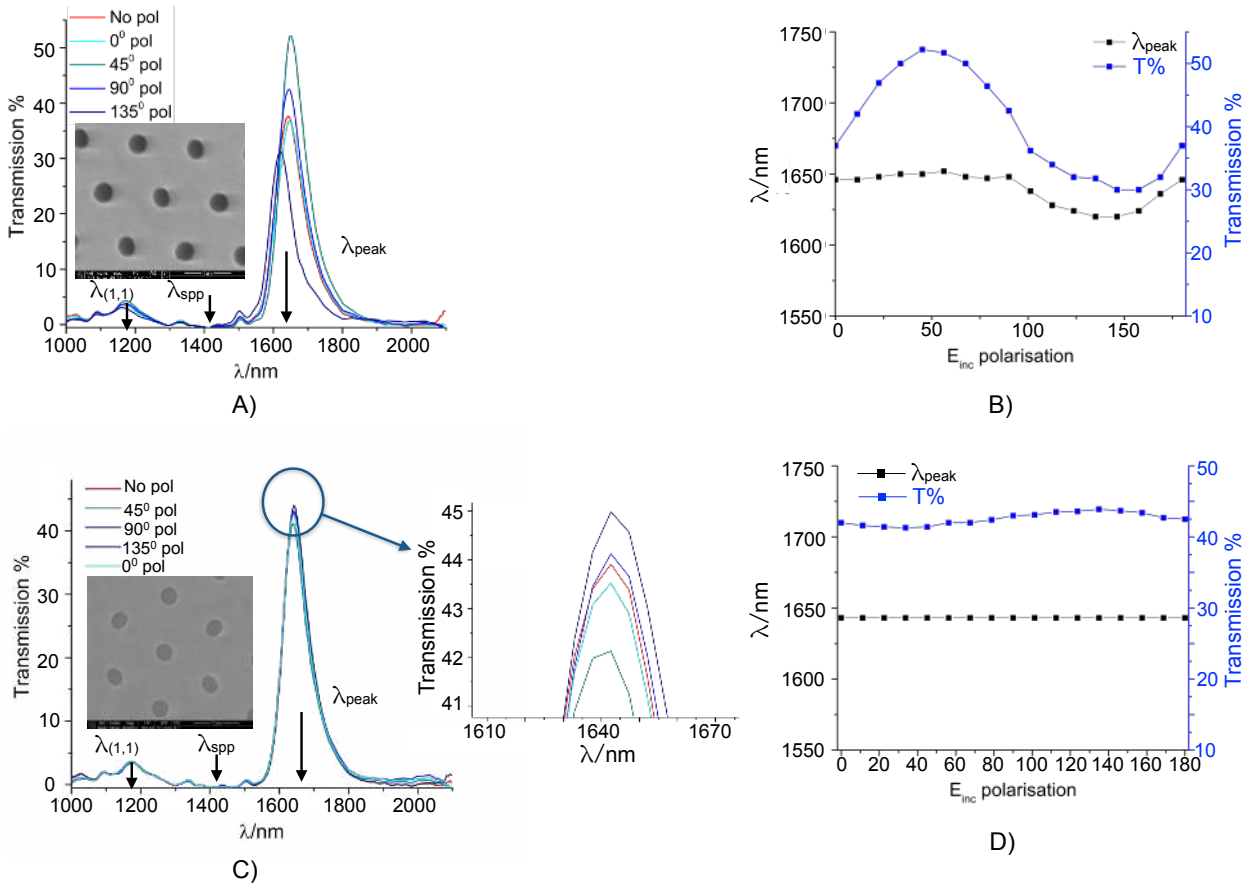

Figure 2: (A) The transmission spectra from the design with ellipses oriented at 135° to the x-axis for $\boldsymbol{E}_{inc}$ at 0°, 45°, 90° and 135° and unpolarised light (red). (B) A variation $\Delta\lambda/\lambda$ of 1.9% and ΔT of 23% is observed. (C) A high transmission of 44% and a narrow linewidth of 79 nm is observed for all $\boldsymbol{E}_{inc}$ polarisations for the design with ellipses oriented at 45° and 135° to the x-axis. (D) The transmission efficiency from this design are polarisation insensitive as $\Delta\lambda/\lambda$ is 0% and ΔT is 2.5%. Both designs have a high out of band rejection.

135°. The transmission data for unpolarised incident light is also shown. A maximum transmission of 53% is observed for $\boldsymbol{E}_{inc}$ polarised at 45° with a narrow linewidth of 92 nm. This can be attributed to the plasmon resonance excited along the shorter axis (b) of the ellipses. However the metasurface is sensitive to the incident polarization - there is a change of 1.9% in wavelength ($\Delta\lambda/\lambda$) and a large change in transmission (ΔT) of 23%, as highlighted in Figure 2(B). However, unlike previously reported plasmonic filters, we observe a suppression of higher order modes with the mode at $\lambda_{(1,1)}$ as small as 4%. The out of band rejection at other wavelengths is below this level. For the device design with the alternate ellipses

oriented at 45° and 135° (unit cell highlighted in the SEM inset in Figure 2(C)) we observe that λ_{peak} is insensitive to variations in the $\boldsymbol{E}_{inc}$ polarisation, and that the transmission remains the same. We observe a very narrow FWHM of 79 nm (Q factor of 26) which is, to the best of our knowledge, the narrowest recorded from a plasmonic metasurface filter.

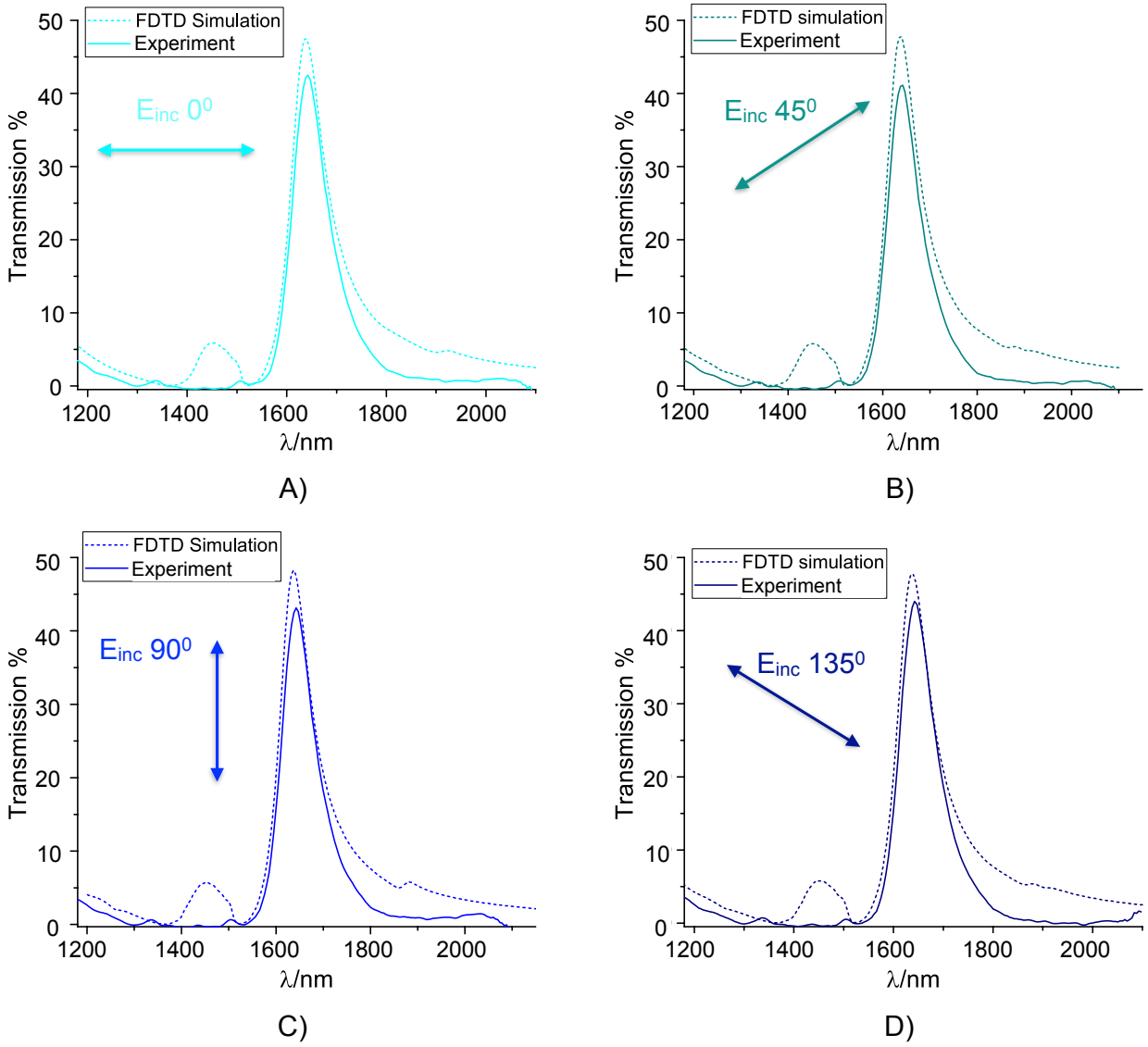

Figure 3: (A), (B), (C) and (D) show the FDTD simulation overlaid with the experimental data for $\boldsymbol{E}_{inc}$ polarisation of 0°, 45°, 90° and 135° respectively, for the design shown in Figure 1(A)(ii).

Figure 2(D) shows the variation in the transmission coefficient as a function of $\boldsymbol{E}_{inc}$. It can be seen that the range is within 2.5% over a rotation of 180°. Similarly, we find

that the variation in the peak transmission wavelength is so small as to be immeasurable with our equipment. The suppression of high order modes and high out of band radiation is also observed for this device design. To demonstrate the robustness and reproducibility of the designs two more devices were fabricated and characterised (see Figure S2 in the Supplementary Information). Our data shows a reproducibility of the characteristics we have described for the two designs.

As seen from the experimental results, the design with the ellipses oriented at 45° and 135° exhibit insensitivity to $\boldsymbol{E}_{inc}$ polarisations while maintaining a high transmission. To understand this phenomenon we carried detailed FDTD simulations. All simulations were performed using the commercially available Lumerical FDTD software using the settings and parameters described in the Methods section. The simulations show excellent agreement with the experimental results for incident light with polarisations of 0°, 45°, 90° and 135°, as shown in Figure 3. For comparison with characterisation of simple circular hole and elliptical hole design, see Supporting Information Figures S3 and S4. From the simulations and experimental data we observe that the transmission peak is asymmetric - indicative of a Fano resonance.[47] The Fano resonance has been observed in plasmonic devices[48,49] and can be induced by symmetry breaking inside the unit cell,[50] interference between dark and bright modes excited by the incident light[51–53] or interference between dipole and quadrupole modes in the structure.[54]

The Fano lineshape from the equation, $I\alpha\frac{\left(q(\frac{\gamma}{2})^2+\omega-\omega_0\right)^2}{(\omega-\omega_0)^2+\left(\frac{\gamma}{2}\right)^2}$, is fitted to both the FDTD simulation and the experimental results in Figure 4. I is the intensity, q is the Fano factor that is slightly larger than 1 in our case, ω is the angular frequency, ω_0 is the angular resonant frequency and γ is the FWHM of the resonant peak. The simulation artefact at 1.44 μm is attributed the (2,1) reflection mode. The (2,1) reflection mode is confined in the substrate. The 2D planar sections in the xz-plane in Figure 4 reveal that at λ_{peak}, higher electric field confinement is observed in elliptical nanoholes than in circular nanhoholes.

Figure 5 illustrates the origin of the Fano resonance, in the sample with the ellipses

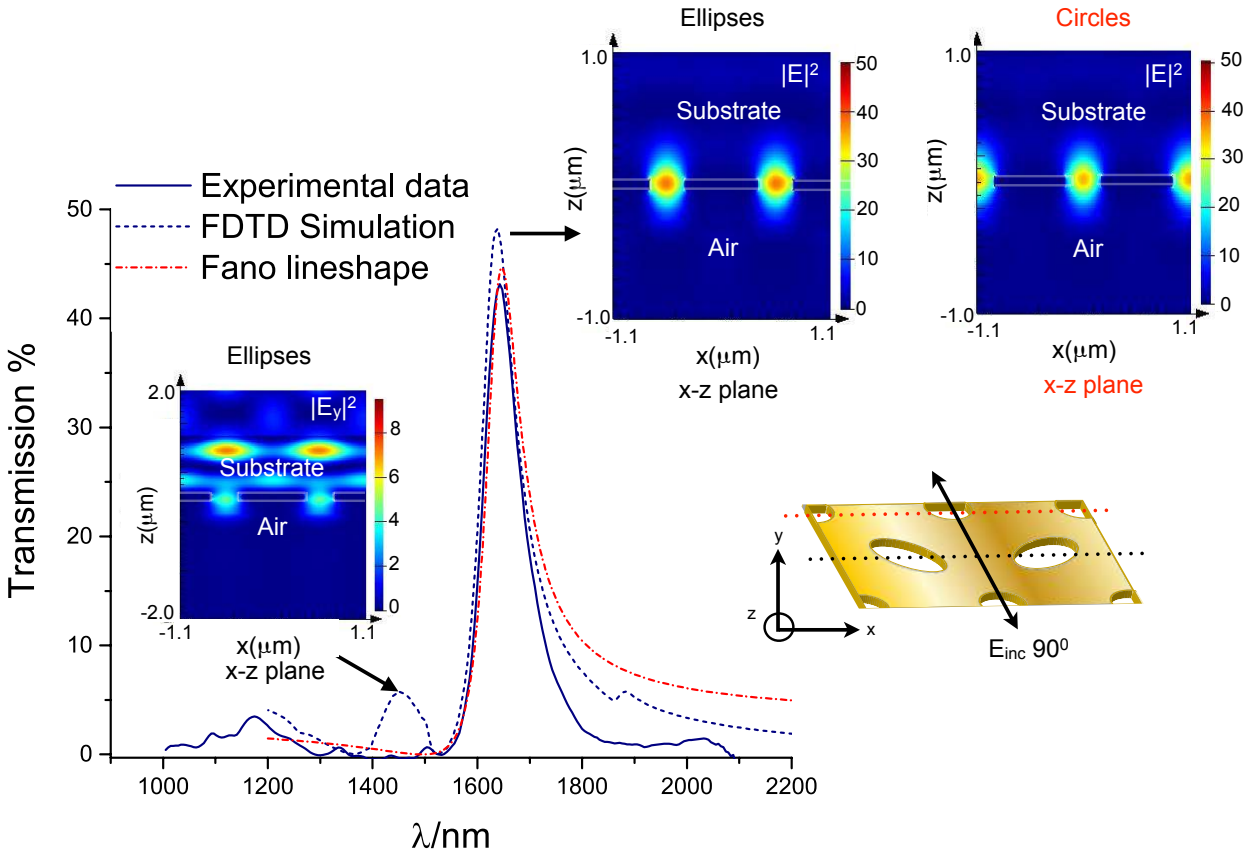

Figure 4: The analytical Fano lineshape compared to the FDTD simulation and the experimental results at $\boldsymbol{E}_{inc} = 90°$. Electric field monitors were placed as indicated in the schematic. At $\lambda_{peak} = 1.642$ μm, $|E|^2$ is higher in elliptical holes than circular holes. The E-field monitor at 1.44 μm shows a reflection into the substrate.

alternately oriented at 45° and 135°, for each incident polarisation. When the incident light is linearly polarized parallel to the y-axis, one would expect, in a circular aperture, to see the electric field reach a maximum in intensity at opposing sides of the circle, on the y-axis, forming a dipole. However, in both of the alternately angled ellipses, the charge distribution forms a quadrupole (see Figure 5(A)(i)). The field pattern looks to be identical (but a mirror image) in both ellipses. The modal changes in the elliptical holes and circular holes were analysed at resonance and off resonance.[55] Off resonance, at $\lambda = 1.68$ μm, the modal distribution in the elliptical holes is a quadrupole that is indicative of a subradiant mode as shown in Figure 5(A)(ii). However, at λ_{peak} the out of plane E-field along the z-axis ($\boldsymbol{E}_z$) shows a quadrupole for the alternating elliptical holes (subradiant mode) and a dipole for

circular holes (super-radiant mode), as seen in Figures 5(A)(iv) and (v). This indicates that $\boldsymbol{E}_{inc}$ cannot excite the dark resonance directly, but only through an interaction involving the dipole resonance that via near-field coupling, excites the sub-radiant mode.[56] When the

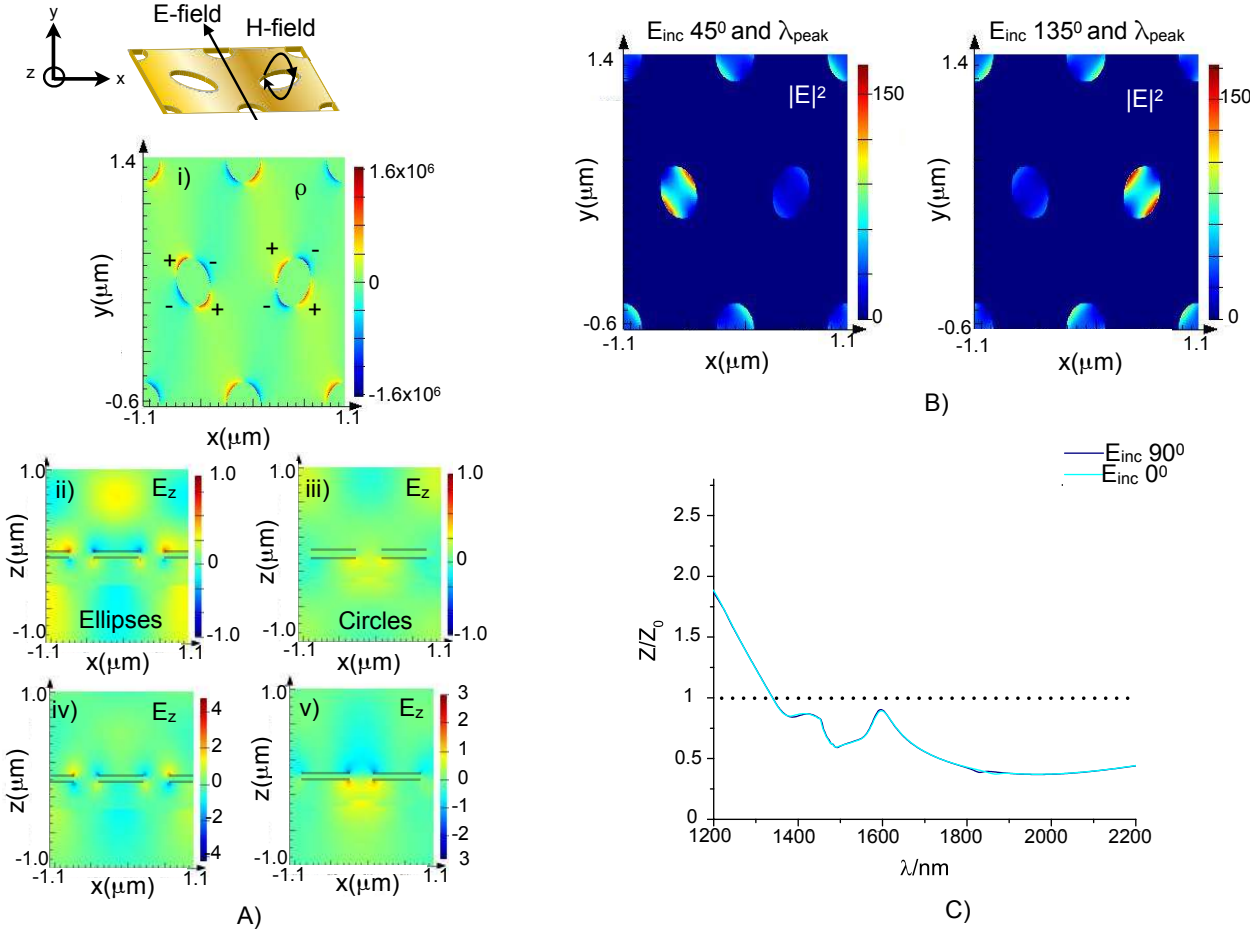

Figure 5: (A) Simulated E-fields for $\boldsymbol{E}_{inc}$ 90°. (i) At λ_{peak}, the surface charge density distribution shows a quadrupolar for the elliptical holes and a dipolar for the circular holes. (ii) and (iii) Simulated out of plane E-fields: $\boldsymbol{E}_z$ field at 1.68 μm (off resonance) that show a clear quadrupole for the elliptical holes only. This is the subradiant mode. However as seen at λ_{peak} in (iv) and (v) the E-field in the ellipses (quadrupole) is the subradiant mode which interacts with the super-radiant mode in the circular holes (dipole), explaining the Fano lineshape. (B) The $|\boldsymbol{E}|^2$ intensity for $\boldsymbol{E}_{inc}$ 45° and 135° show that only one ellipse contributes to the EOT which results in asymmetry in the design that leads to a Fano lineshape. (C) Calculated normalized impedance ($Z/Z0$) plots at $\boldsymbol{E}_{inc}$ 0° and 90° that shows at λ_{peak}, the value is nearly 1.

incident light is linearly polarized parallel to the y-axis, i.e. $\boldsymbol{E}_{inc}$ at 0° polarisation, the E-fields in the ellipses are opposite to what is discussed for $\boldsymbol{E}_{inc}$ 90°. For $\boldsymbol{E}_{inc}$ at 45° and 135°,

only one of the ellipses has a modal confinement contributing to the EOT as shown in Figure 5(B). This creates asymmetry in the structure and hence we observe the Fano resonance for these polarisations of incident light. Figures S5 and S6 in the Supplementary Information show the difference in mode confinement in the ellipses for $\boldsymbol{E}_{inc}$ at 45° and 135°, respectively. We also calculated the optical impedance of the device from the s-parameters extracted with incident light polarized along the x and y axis. A normalised optical impedance (Z/Z_0: where Z_0 is the impedance of free space) of unity would indicate high efficiency transmission with no reflection from the metasurface. Due to the asymmetry of the design, S_{11} and S_{21} were calculated with the light incident through the substrate and S_{22} and S_{12} were calculated with light incident from the opposite direction (through air).[57,58] The optical impedance z is calculated from Equation 2:

$$z^2 = \frac{T_{12}}{T_{21}} = \frac{(1+S_{11})(1+S_{22}) - S_{21}S_{12}}{(1-S_{11})(1+S_{22}) - S_{12}S_{21}} \tag{2}$$

This is normalized to Z_0 for $\boldsymbol{E}_{inc}$ 0° and 90° with the plots shown in Figure 5(C). For both polarisations of incident light we observe that at resonance (1.61 μm for the S parameter calculation) the value is almost 1.

In conclusion, we have demonstrated a novel plasmonic metasurface design with arrays of elliptical and circular nanoholes in a metallic film to obtain an unprecedented high transmission efficiency of 44% and narrow FWHM of 79 nm. Polarisation insensitivity is observed with a $\Delta\lambda/\lambda$ of 0 and ΔT of 2.5%. The experimental transmission spectra are matched well with FDTD simulations. We have shown that the narrow linewidth is due to an interplay between the Fano resonance and the EOT. The Fano resonance arises due to the symmetry breaking of the design with respect to the $\boldsymbol{E}_{inc}$ polarization: being anti-symmetric in the x-axis and symmetric in the y-axis, leading to dark modes interacting with the incident light. At $\boldsymbol{E}_{inc}$ of 0° and 90° a negligible mismatch in optical impedance with the free space was observed around λ_{peak} with the normalized impedance value being almost 1. The narrow

linewidth and high out of band rejection is comparable to state-of-the-art dichroic filters which makes our metasurface filters ideal for integration with appropriate photodetectors.

Methods

Fabrication

The substrate used is a borosilicate glass slide of dimensions 20 mm × 20 mm and thickness 515 μm. A lift-off process was employed to obtain the elliptical and circular nanohole designs. A bilayer of polymethyl methacrylate (PMMA) was spin coated onto the substrates and the designs patterned into the resist using a Vistec VB6 electron beam lithography (EBL) tool. 80 nm of Au is deposited using a Plassys electron beam evaporator and the sample placed in warm acetone maintained at 50° overnight. After lift-off, the sample was then cleaned in acetone and isopropyl alcohol. The devices were annealed in a furnace in an atmosphere of N_2 gas at a temperature of 605° for 3 hours. After annealing, 300 nm of silicon dioxide was deposited on top of the Au layer using a plasma enhanced chemical vapour deposition (PECVD) process. The addition of the cap layer enhances the transmission.[30]

Simulation setup

The plasmonic filter simulations are set up as follows: a 80 nm gold layer was placed between a semi-infinite borosilicate layer and a 300 nm silicon dioxide (SiO_2) cap layer. The gold was patterned with the two different unit cell design (discussed in Figure 1(A)) and the silicon dioxide cap layer was patterned with "etch" holes to replicate the cap layer topography after deposition of silicon dioxide. A mesh grid with a maximum cell size of 5 nm was defined in the vicinity of the holes. For $\boldsymbol{E}_{inc}$ of 0° and 90°, anti-symmetric and symmetric boundary conditions were used, respectively, to form the unit cells highlighted in Figure 1(A), and perfectly matched layers (PML) were used in the z boundaries. For $\boldsymbol{E}_{inc}$ of 45° and 135° polarisation, periodic boundary conditions were used in the x and y axes. The gold parameters were selected using a plasma resonance (ω_p) of 1.37 × 10^{16} rad/s and

collision frequency (ω_c) of 1.224×10^{16} rad/s with the refractive index (η) of borosilicate glass substrate as 1.52 and SiO_2 cap of 1.49 (extrapolated from spectroscopic ellipsometry analysis). Steep angle boundary conditions were used in the FDTD simulation to absorb all the light at the boundaries and prevent any spurious reflections. The gold surface was illuminated by a 1.2 μm to 2.1 μm plane-wave source from within the substrate and the transmission spectra were recorded by a monitor placed on the opposite side of the metal film.

Acknowledgement

The authors thank the James Watt Nanofabrication Centre (JWNC) staff for their expertise and assistance in fabrication processes. This work was supported by the Engineering and Physical Sciences Research Council of the United Kingdom, Grant Nos. EP/M01326X/1 and EP/J018678/1.

Supporting Information Available

A file called Supplementary Information is included. This file contains simulation results of the variation of metal thickness on the proposed design for $\boldsymbol{E}_{inc}$ at 0∘ and 90°. A comparison between the proposed design and simple circular holes and elliptical holes only design is shown. The simulations supporting the origin of Fano resonance when $\boldsymbol{E}_{inc}$ is 45° and 135° is explicitly shown.

This material is available free of charge via the Internet at `http://pubs.acs.org/`.

References

(1) Ellenbogen, T.; Seo, K.; Crozier, K. B. Chromatic plasmonic polarizers for active visible color filtering and polarimetry. *Nano Lett.* **2012**, *12*, 1026–1031.

(2) McCrindle, I. J. H. Structured Photonic Materials for Multi-Spectral Imaging Applications. Ph.D. thesis, 2015.

(3) Yokogawa, S.; Burgos, S. P.; Atwater, H. A. Plasmonic color filters for CMOS image sensor applications. *Nano Lett.* **2012**, *12*, 4349–4354.

(4) Alvarez, J.; Jaffré, A.; Renard, C.; Cherkasin, N.; Molière, T.; Vincent, L.; Hamouche, R.; Yam, V.; Fossard, F.; Kleider, J. P.; Mencaraglia, D.; Bouchier, D. Nano-Structures for Optics and Photonics. *NATO Sci. Peace Secur. Ser. B Phys. Biophys.* **2015**, *68*, 485–486.

(5) Brongersma, M. L. Introductory lecture: nanoplasmonics. *Faraday Discuss.* **2015**, *178*, 9–36.

(6) Chen, H.-T.; Taylor, A. J.; Yu, N. A review of metasurfaces: physics and applications. *Rep. Prog. Phys.* **2016**, 76401.

(7) Gramotnev, D. K.; Bozhevolnyi, S. I. Plasmonics beyond the diffraction limit. *Nat. Photonics* **2010**, *4*, 83–91.

(8) Kristensen, A.; Yang, J. K. W.; Bozhevolnyi, S. I.; Link, S.; Nordlander, P.; Halas, N. J.; Mortensen, N. A. Plasmonic colour generation. *Nat. Rev. Mater.* **2016**, *2*, 16088.

(9) Maier, S. A. *Plasmonics: fundamentals and applications*; Springer Science & Business Media, 2007.

(10) Schmidt, M. A.; Lei, D. Y.; Wondraczek, L.; Nazabal, V.; Maier, S. A. Hybrid nanoparticle–microcavity-based plasmonic nanosensors with improved detection resolution and extended remote-sensing ability. *Nat. Commun.* **2012**, *3*, 1108.

(11) Tame, M.; McEnery, K.; Oezdemir, S.; Lee, J.; Maier, S.; Kim, M. Quantum plasmonics. *Nat. Phys.* **2013**, *9*, 329–340.

(12) Ozbay, E. Plasmonics: Merging Photonics and Electronics at Nanoscale Dimensions. *Science* **2006**, *311*, 189–193.

(13) Kildishev, A. V.; Boltasseva, A.; Shalaev, V. M. Planar Photonics with Metasurfaces. *Science* **2013**, *339*.

(14) Yu, N.; Capasso, F. Flat optics with designer metasurfaces. *Nat. Mater.* **2014**, *13*, 139–150.

(15) Meinzer, N.; Barnes, W. L.; Hooper, I. R. Plasmonic meta-atoms and metasurfaces. *Nat. Photonics* **2014**, *8*, 889–898.

(16) Xia, F.; Wang, H.; Xiao, D.; Dubey, M.; Ramasubramaniam, A. Two-dimensional material nanophotonics. *Nat. Photonics* **2014**, *8*, 899–907.

(17) Lin, D.; Fan, P.; Hasman, E.; Brongersma, M. L. Dielectric gradient metasurface optical elements. *Science* **2014**, *345*, 298 LP – 302.

(18) Liu, G.; Fu, G.; Liu, Z.; Huang, Z.; Chen, J. Partially hollowed ultra-thin dielectric meta-surface for transmission manipulation. *Opt. Express* **2016**, *24*, 20580.

(19) Zhao, Y.; Alù, A. Manipulating light polarization with ultrathin plasmonic metasurfaces. *Phys. Rev. B* **2011**, *84*, 205428.

(20) Bergman, D.; Strelniker, Y. Magnetotransport in conducting composite films with a disordered columnar microstructure and an in-plane magnetic field. *Phys. Rev. B* **1999**, *60*, 13016–13027.

(21) Barnes, W. L. Surface plasmon polariton length scales: a route to sub-wavelength optics. *J. Opt. A-Pure Appl. Op.* **2006**, *8*, S87–S93.

(22) Lin, L.; Roberts, A. Light transmission through nanostructured metallic films: coupling between surface waves and localized resonances. *Opt. Express* **2011**, *19*, 2626–2633.

(23) Ebbesen, T. W.; Lezec, H. J.; Ghaemi, H. F.; Thio, T.; Wolff, P. A. Extraordinary optical transmission through sub-wavelength hole arrays. *Nature* **1998**, *391*, 667–669.

(24) De Abajo, F. J. G. Colloquium: Light scattering by particle and hole arrays. *Rev. Mod. Phys.* **2007**, *79*, 1267–1290.

(25) Martín-Moreno, L.; García-Vidal, F. J.; Lezec, H. J.; Pellerin, K. M.; Thio, T.; Pendry, J. B.; Ebbesen, T. W. Theory of Extraordinary Optical Transmission through Subwavelength Hole Arrays. *Phys. Rev. Lett.* **2001**, *86*, 1114–1117.

(26) Ruan, Z.; Qiu, M. Enhanced transmission through periodic arrays of subwavelength holes: the role of localized waveguide resonances. *Phys. Rev. Lett.* **2006**, *96*, 233901.

(27) Genet, C.; Ebbesen, T. W. Light in tiny holes. *Nature* **2007**, *445*, 39–46.

(28) Glushko, O.; Brunner, R.; Meisels, R.; Kalchmair, S.; Strasser, G. Extraordinary transmission in metal hole array-photonic crystal hybrid structures. *Opt. Express* **2012**, *20*, 17174.

(29) Barnes, W. L.; Dereux, A.; Ebbesen, T. W. Surface plasmon subwavelength optics. *Nature* **2003**, *424*, 824–30.

(30) Chen, Q.; Cumming, D. R. S. High transmission and low color cross-talk plasmonic color filters using triangular-lattice hole arrays in aluminum films. *Opt. Express* **2010**, *18*, 14056.

(31) McCrindle, I. J. H.; Grant, J. P.; Gouveia, L. C. P.; Cumming, D. R. S. Infrared plasmonic filters integrated with an optical and terahertz multi-spectral material. *Phys. Status Solidi A* **2015**, *212*, 1625–1633.

(32) Przybilla, F.; Degiron, a.; Laluet, J.-Y.; Genet, C.; Ebbesen, T. W. Optical transmission in perforated noble and transition metal films. *J. Opt. A: Pure Appl. Opt.* **2006**, *8*, 458–463.

(33) Garcia-Vidal, F. J.; Martin-Moreno, L.; Ebbesen, T. W.; Kuipers, L. Light passing through subwavelength apertures. *Rev. Mod. Phys.* **2010**, *82*, 729–787.

(34) Khurgin, J. B. How to deal with the loss in plasmonics and metamaterials. *Nat. Nanotechnol.* **2015**, *10*, 2–6.

(35) Xu, T.; Wu, Y.-K.; Luo, X.; Guo, L. J. Plasmonic nanoresonators for high-resolution colour filtering and spectral imaging. *Nat. Commun.* **2010**, *1*, 59.

(36) Gibson, G. M.; Sun, B.; Edgar, M. P.; Phillips, D. B.; Hempler, N.; Maker, G. T.; Malcolm, G. P. A.; Padgett, M. J. Real-time imaging of methane gas leaks using a single-pixel camera. *Opt. Express* **2017**, *25*, 2998–3005.

(37) Guo, R.; Hakala, T. K.; Törmä, P. Geometry dependence of surface lattice resonances in plasmonic nanoparticle arrays. *Phys. Rev. B* **2017**, *95*, 155423.

(38) Ekşioğlu, Y.; Cetin, A. E.; Petráček, J. Optical Response of Plasmonic Nanohole Arrays: Comparison of Square and Hexagonal Lattices. *Plasmonics* **2016**, *11*, 851–856.

(39) Strelniker, Y. M. Theory of optical transmission through elliptical nanohole arrays. *Phys. Rev. B* **2007**, *76*, 085409.

(40) Gordon, R.; Brolo, A.; McKinnon, A.; Rajora, A.; Leathem, B.; Kavanagh, K. Strong polarization in the optical transmission through elliptical nanohole arrays. *Phys. Rev. Lett.* **2004**, *92*, 037401.

(41) Elliott, J.; Smolyaninov, I. I.; Zheludev, N. I.; Zayats, A. V. Polarization control of optical transmission of a periodic array of elliptical nanoholes in a metal film. *Opt. Lett.* **2004**, *29*, 1414–1416.

(42) Cao, T.; Wang, S.; Jiang, W. Tunable metamaterials using a topological insulator at near-infrared regime. *RSC Adv.* **2013**, *3*, 19474–19480.

(43) Chakrabarty, A.; Wang, F.; Minkowski, F.; Sun, K.; Wei, Q.-H. Cavity modes and their excitations in elliptical plasmonic patch nanoantennas. *Opt. Express* **2012**, *20*, 11615–24.

(44) Cervantes Tellez, G. A.; Hassan, S.; Tait, R. N.; Berini, P.; Gordon, R. Atomically flat symmetric elliptical nanohole arrays in a gold film for ultrasensitive refractive index sensing. *Lab Chip* **2013**, *13*, 2541–2546.

(45) Pacifici, D.; Lezec, H. J.; Sweatlock, L. A.; Walters, R. J.; Atwater, H. A. Universal optical transmission features in periodic and quasiperiodic hole arrays. *Opt. Express* **2008**, *16*, 9222–9238.

(46) Burgos, S. P.; Yokogawa, S.; Atwater, H. A. Color imaging via nearest neighbor hole coupling in plasmonic color filters integrated onto a complementary metal-oxide semiconductor image sensor. *ACS Nano* **2013**, *7*, 10038–10047.

(47) Fano, U. Effects of configuration interaction on intensities and phase shifts. *Phys. Rev.* **1961**, *124*, 1866–1878.

(48) Luk'yanchuk, B.; Zheludev, N. I.; Maier, S. A.; Halas, N. J.; Nordlander, P.; Giessen, H.; Chong, C. T. The Fano resonance in plasmonic nanostructures and metamaerials. *Nat. Mater.* **2010**, *9*, 707–715.

(49) Genet, C.; Van Exter, M. P.; Woerdman, J. P. Fano-type interpretation of red shifts and red tails in hole array transmission spectra. *Opt. Commun.* **2003**, *225*, 331–336.

(50) Sonnefraud, Y.; Verellen, N.; Sobhani, H.; Vandenbosch, G. A. E.; Moshchalkov, V. V.; Van Dorpe, P.; Nordlander, P.; Maier, S. A. Experimental realization of subradiant, superradiant, and fano resonances in ring/disk plasmonic nanocavities. *ACS Nano* **2010**, *4*, 1664–1670.

(51) Fan, P.; Yu, Z.; Fan, S.; Brongersma, M. L. Optical Fano resonance of an individual semiconductor nanostructure. *Nat. Mater.* **2014**, *13*, 471–475.

(52) Ferry, V. E.; Hentschel, M.; Alivisatos, A. P. Circular Dichroism in Off-Resonantly Coupled Plasmonic Nanosystems. *Nano Lett.* **2015**, *15*, 8336–8341.

(53) Gomez, D. E.; Teo, Z. Q.; Altissimo, M.; Davis, T. J.; Earl, S.; Roberts, A. The Dark Side of Plasmonics. *Nano lett.* **2013**, *13*, 3722–3728.

(54) Wu, C.; Arju, N.; Kelp, G.; Fan, J. A.; Dominguez, J.; Gonzales, E.; Tutuc, E.; Brener, I.; Shvets, G. Spectrally selective chiral silicon metasurfaces based on infrared Fano resonances. *Nat. Commun.* **2014**, *5*, 3892.

(55) Gallinet, B.; Martin, O. J. F. Influence of electromagnetic interactions on the line shape of plasmonic fano resonances. *ACS Nano* **2011**, *5*, 8999–9008.

(56) Giannini, V.; Francescato, Y.; Amrania, H.; Phillips, C. C.; Maier, S. A. Fano Resonances in Nanoscale Plasmonic Systems: A Parameter-Free Modeling Approach. *Nano Lett.* **2011**, *11*, 2835–2840.

(57) Smith, D. R.; Schultz, S.; Markoš, P.; Soukoulis, C. M. Determination of effective permittivity and permeability of metamaterials from reflection and transmission coefficients. *Phys. Rev. B* **2002**, *65*, 195104.

(58) Smith, D. R.; Vier, D. C.; Koschny, T.; Soukoulis, C. M. Electromagnetic parameter retrieval from inhomogeneous metamaterials. *Phys. Rev. E: Stat., Nonlinear, Soft Matter Phys.* **2005**, *71*, 1–11.

Graphical TOC Entry

Some journals require a graphical entry for the Table of Contents. This should be laid out "print ready" so that the sizing of the text is correct.
Inside the `tocentry` environment, the font used is Helvetica 8 pt, as required by *Journal of the American Chemical Society*.
The surrounding frame is 9 cm by 3.5 cm, which is the maximum permitted for *Journal of the American Chemical Society* graphical table of content entries. The box will not resize if the content is too big: instead it will overflow the edge of the box.
This box and the associated title will always be printed on a separate page at the end of the document.

ToC: Ultra-narrow linewidth polarization-insensitive filter using a symmetry-breaking selective plasmonic metasurface

Yash D. Shah,* James Grant, Danni Hao, Mitchell Kenney, Vincenzo Pusino, and David R. S. Cumming†

Microsystems Technology group, Electronics and Nanoscale engineering, Department of Engineering, University of Glasgow, Glasgow, UK.

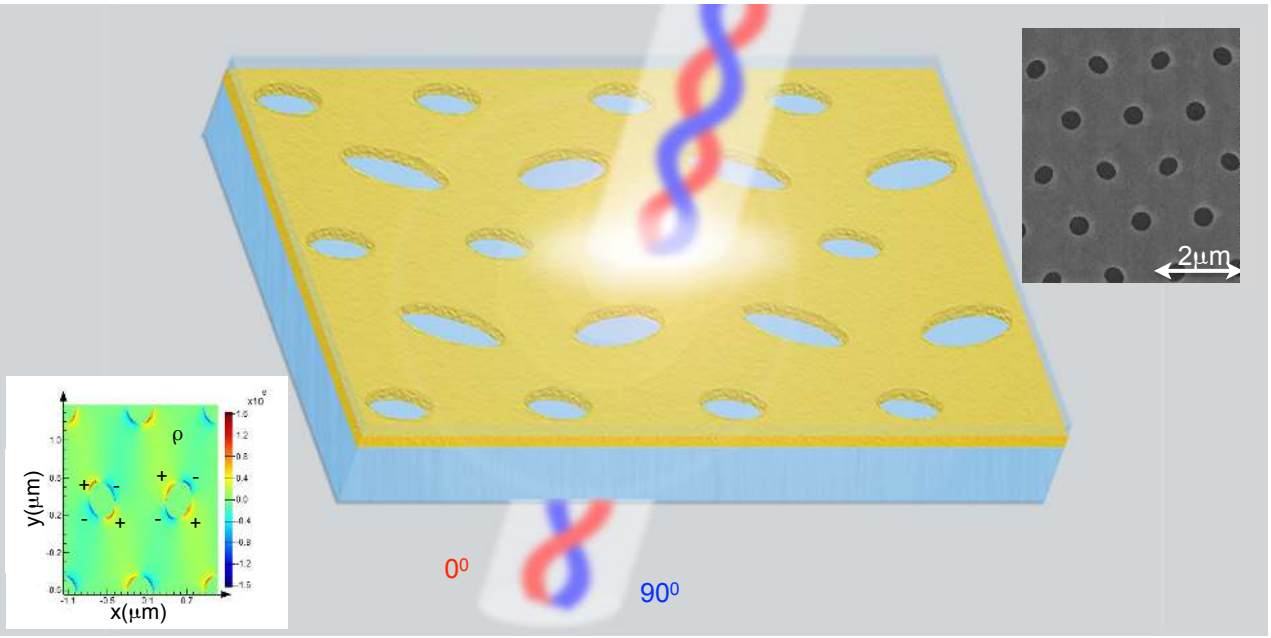

*Electronic address: YashDiptesh.Shah@glasgow.ac.uk

†Electronic address: david.cumming.2@glasgow.ac.uk